2017-12-01

Evaporated Aluminum Fluoride as a Barrier Layer to Retard Oxidation of Aluminum Mirrors

Margaret Miles
Brigham Young University

Evaporated Aluminum Fluoride as a Barrier Layer to Retard Oxidation of Aluminum Mirrors

Margaret Miles

A thesis submitted to the faculty of
Brigham Young University
in partial fulfillment of the requirements for the degree of

Master of Science

R. Steven Turley, Chair
David D. Allred
Justin B. Peatross

Department of Physics and Astronomy

Brigham Young University

ABSTRACT

Evaporated Aluminum Fluoride as a Barrier Layer to Retard Oxidation
of Aluminum Mirrors

Margaret Miles
Department of Physics and Astronomy, BYU
Master of Science

The aluminum oxide growth rate for aluminum protected with 2.4 nm of aluminum fluoride has been determined. We show that a 2.4 nm aluminum fluoride layer does not prevent aluminum from oxidation but does significantly retard the oxide growth – decreasing the oxide layer thickness from 1 nm in less than an hour to 0.9 nm over 116 hours. Additionally, the optical constants for aluminum oxide growing under an aluminum fluoride barrier layer have been determined – showing an increase in absorption at high energies for Al_2O_3 forming at room temperature as compared to highly ordered Al_2O_3 formed at high temperatures.

Keywords: UV astronomy, aluminum fluoride, aluminum oxide growth rate, LUVOIR, thin film

ACKNOWLEDGEMENTS

This research would not have been possible without the help of Steven Turley, David Allred, and John Ellsworth of the BYU physics department.

This research was funded in part by the NASA Space Grant Consortium.

Table of Contents

List of Tables

List of Figures

Chapter 1: Introduction

1.1 Background: Interest in the Ultraviolet

The extreme ultraviolet wavelength range contains an abundance of spectral lines from common elements essential to the study of astrophysics (Fig. 1).[1] The O VI 103.2 nm and 103.8 nm doublet lines allow a study of the warm-hot intergalactic medium.[2] The C III 97.7 nm line aids in the investigation of supernovae explosion dynamics and emission nebulae.[2] The hydrogen Lyman series 91.2 nm – 121.6 nm, C II 103.7 nm, and N II 108.5 nm lines provide information about the characteristics of exoplanet atmospheres.[3]

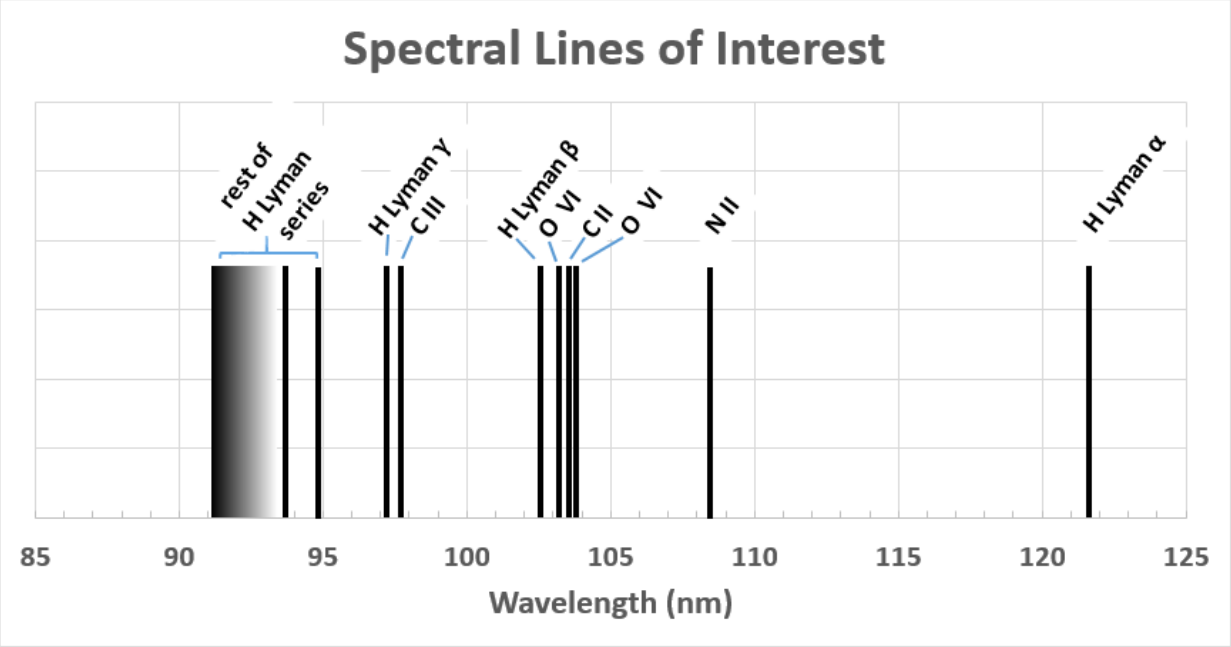

Figure 1: Astrophysical spectral lines of interest in the ultraviolet wavelength range.

Since Earth's atmosphere blocks most ultraviolet radiation, observations of these spectral lines require telescopes in space. Therefore, the need for space telescope mirrors that reflect well in the ultraviolet range has grown in recent years.[4,5,6]

1.2 Motivation: the Necessity of Preventing Oxidation of an Aluminum Mirror

The Large UV/Optical/IR Surveyor (LUVOIR) to be considered for priority in NASA's 2020 decadal survey will have an 8-16 meter telescope mirror with a surface able to reflect extreme ultraviolet wavelengths as well as visible light and infrared radiation.[7] Since NASA is currently investing in technologies essential for the launch of LUVOIR, broadband reflective coatings for the telescope mirror are being developed.[8,9] Aluminum is an excellent candidate for broadband reflection[10]; however, aluminum mirrors oxidize upon contact with Earth's atmosphere. This is a problem because a layer of aluminum oxide significantly decreases reflectance in the ultraviolet[11]. Whereas aluminum has greater than 90% reflectance down to 100 nm, which is

dramatically higher in the ultraviolet wavelength range than other commonly used metals (Fig. 2), that reflectance decreases by 20% with the addition of even 1 nm of aluminum oxide (Fig. 3).

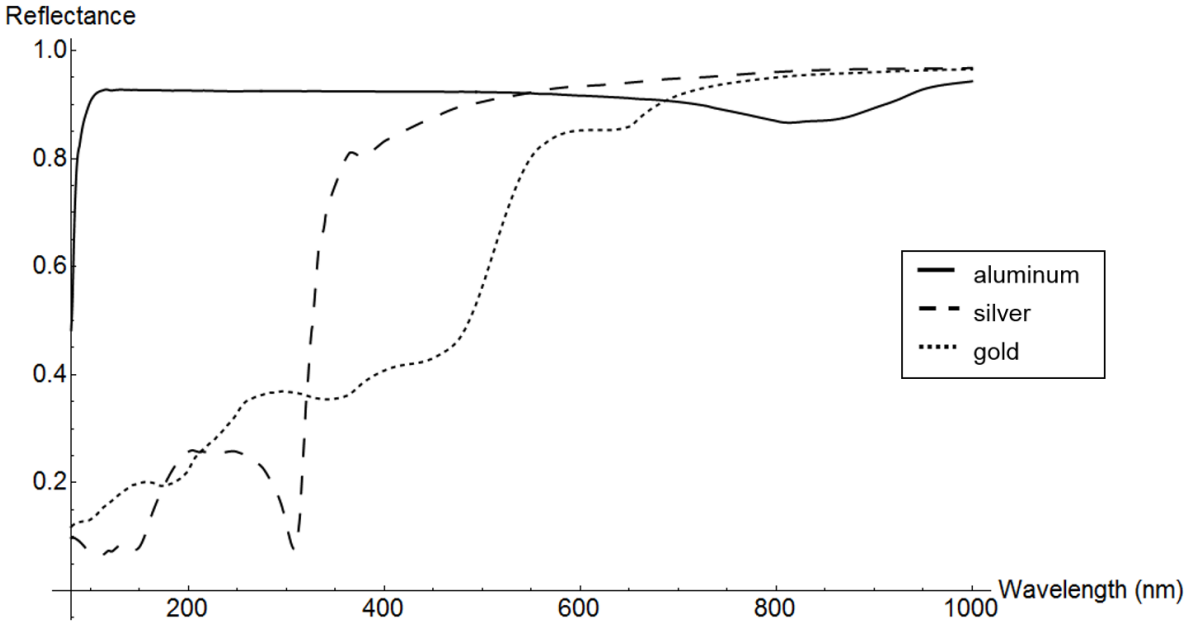

Figure 2: Broadband reflectance of thick-film aluminum on a silicon substrate compared to other common mirror coatings on the same substrate. Reflectances were calculated using the Parratt method employing literature optical constants[12].

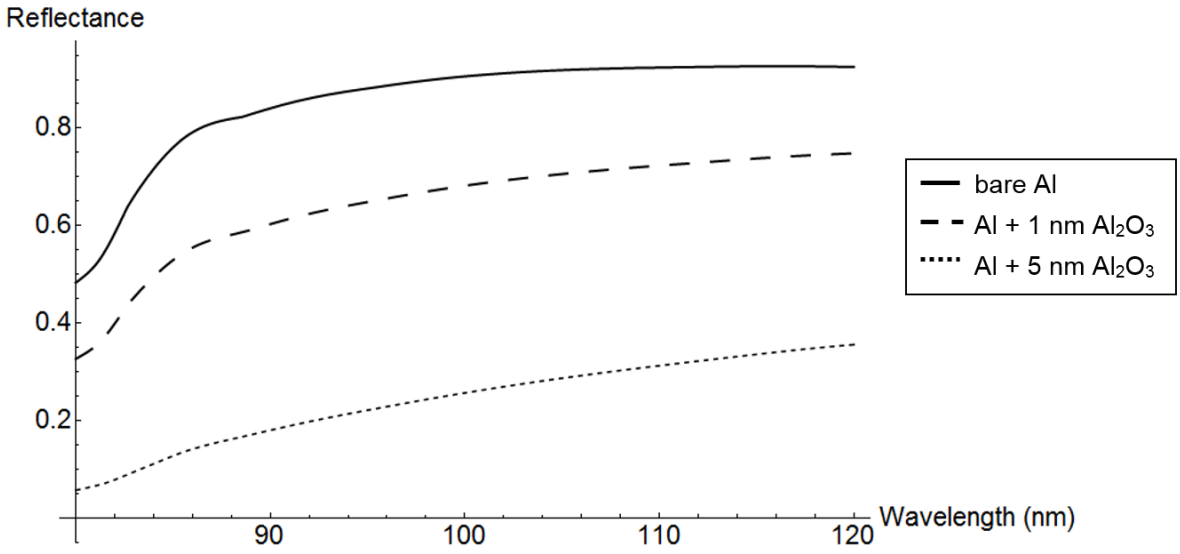

Figure 3: Decrease in reflectance over far ultraviolet wavelengths as a function of aluminum oxide growth.

To circumvent this problem, several solutions have been contemplated. First, the mirror could be coated with aluminum in space[1,13] or coated under vacuum and then kept under vacuum until placed in space. Aside from the tremendous technical difficulty involved in either of these solutions, there are conditions where oxidation of the aluminum could still occur in orbit.[14] Another contemplated solution is to use a material other than aluminum for the mirror. In order to decide if an alternate material should be used, it is necessary to know if the reflectance sacrificed by using another material would be greater than the reflectance sacrificed as aluminum oxidizes. This would require knowing how fast the aluminum oxide layer grows. Another possibility is to coat the aluminum mirror with a substance that retards aluminum oxidization. This substance could either be an opaque layer to be etched away once the mirror is in space[15] or a weakly absorbing layer to remain on the mirror while the telescope is in use.[16] However, oxidation of the aluminum could occur between the deposition of the aluminum and the deposition of the second layer. Additionally, oxidation could occur if the second layer is not completely impervious to water vapor or air.[17] Moreover, coating the aluminum mirror could increase the mirror's surface roughness, reducing reflectance due to scattering.[18] Therefore, for a mirror coated with a weakly absorbing layer to be seriously considered for the LUVOIR mission, further investigation is required.

1.3 Prior Work

To prevent oxidation of aluminum mirrors, metal fluorides have been deposited in vacuum systems where aluminum and then a metal fluoride can be deposited while the substrate is continuously under vacuum. Specifically, lithium fluoride (LiF), magnesium fluoride (MgF_2). and aluminum fluoride (AlF_3) have shown promise as layers that are weakly absorbing in the ultraviolet range that can impede aluminum oxide growth. Although LiF has the largest

transparency range, its deposition generally results in a rougher surface which decreases reflectance. Additionally, its hygroscopic nature can foster oxide growth.[18] Aluminum fluoride appears to have the smoothest surface after deposition[18] and shows promise as a protective layer. Aluminum fluoride could be used as the sole barrier layer deposited on aluminum or it could be used in conjunction with LiF to form a multilayer barrier.

1.4 Present Work

In this research, we investigated the ability of AlF_3 to protect aluminum mirrors against oxidation while preserving the reflective ability of aluminum in the ultraviolet wavelength range. Specifically, we thermally evaporated 22 nm of Al and coated it with a 2.4 nm AlF_3 barrier layer to impede oxidation. We then used ellipsometry to measure growth of an Al_2O_3 layer between the Al and the AlF_3 over time. Results showed a significant decrease in oxide growth as compared with oxidation of bare Al. We also used atomic force microscopy (AFM) measurements to ascertain the roughness of the sample surface: we determined that the roughness is low enough to allow good reflectance of the Al mirror beneath the AlF_3 layer. Finally, we modeled reflectance of ultraviolet wavelengths for Al coated with AlF_3 to show that coating the Al mirror with AlF_3 does not yield the same decrease in reflectance caused by growth of Al_2O_3.

Chapter 2: Methodology

2.1 Evaporation of thin film aluminum and aluminum fluoride

To evaporate thin film aluminum protected by aluminum fluoride, we used a Denton model 502A thermal evaporator with two independently heated sources and an oil diffusion pump system (Fig. 4). Aluminum wire was evaporated by resistive heating of a tungsten filament followed by evaporation of aluminum fluoride pellets (prepared by Pure Tech, Inc.) using a tungsten boat. A silicon wafer coated with CVD-deposited silicon nitride was used as the substrate. The substrate was prepared in a clean room environment and cleaved in the lab to a 6 cm x 2 cm size before being affixed to a rotating sample stage. An Inficon quartz crystal monitor linked to a shutter allowed for systematic deposition of controlled thicknesses.

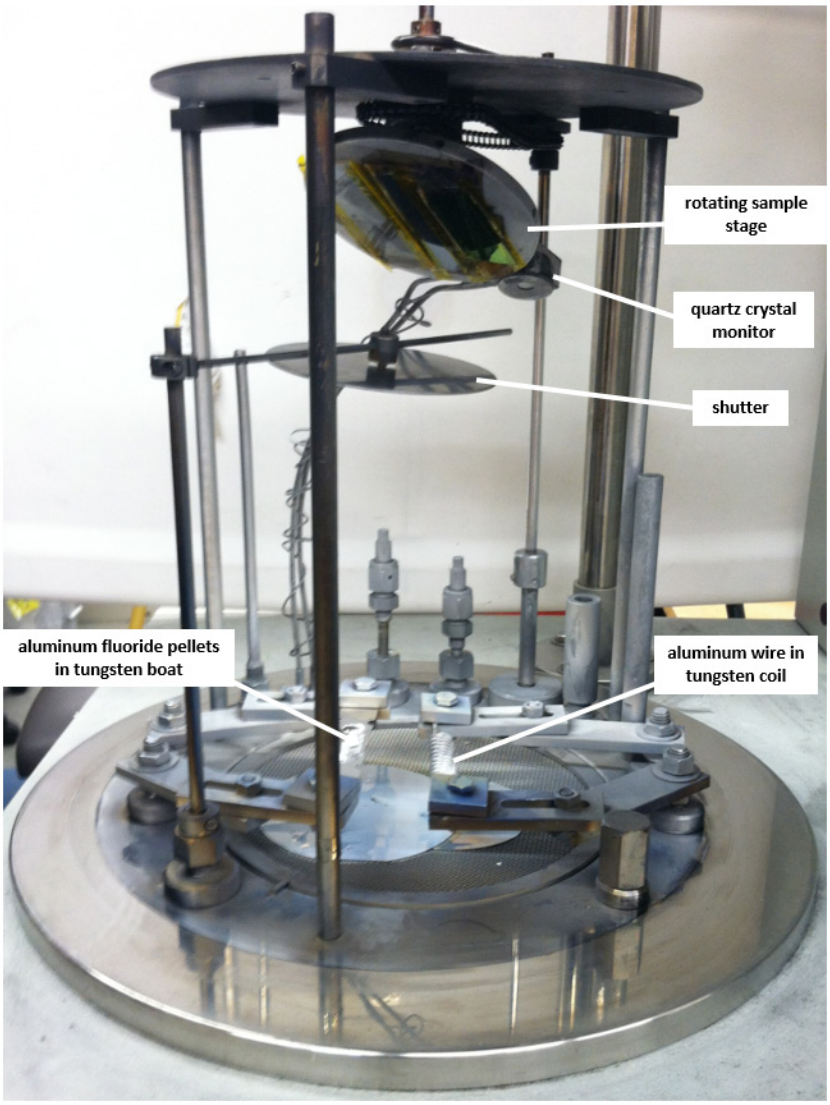

Figure 4: Thermal evaporator setup.

Prior to deposition, the deposition chamber was pumped down to the mid 10^{-6} torr range and was at room temperature. During deposition, the pressure rose to 10^{-4} torr – presumably due to release of water vapor from the chamber as the chamber walls were heated radiatively.

To limit the amount of oxygen contacting the aluminum, the aluminum was deposited as rapidly as possible (at a deposition rate of approximately 5-10 nm/s) and the time between the evaporation of aluminum and evaporation of aluminum fluoride was minimized (less than 10 s).

2.2 Data Collection

2.2.a Ellipsometry

The sample was removed from vacuum conditions and analyzed using ellipsometry. Successive ellipsometric data sets were collected at logarithmically increasing time intervals to determine the trend in Al_2O_3 growth. Ellipsometry data was taken using a John A. Woollam M2000 variable-angle spectroscopic ellipsometer with photon energies of 1.2 eV - 7 eV at incident angles of 50º -80º. During data collection, light initiating from one arm of the ellipsometer reflected off the sample and was then detected by the other arm of the ellipsometer – which allowed the ratio of light polarizations (perpendicular and parallel) in the reflected light to be measured. This light polarization ratio was graphed as a complex number in polar coordinates with $\tan(\psi)$ as the magnitude and Δ as the angle (Fig. 5).

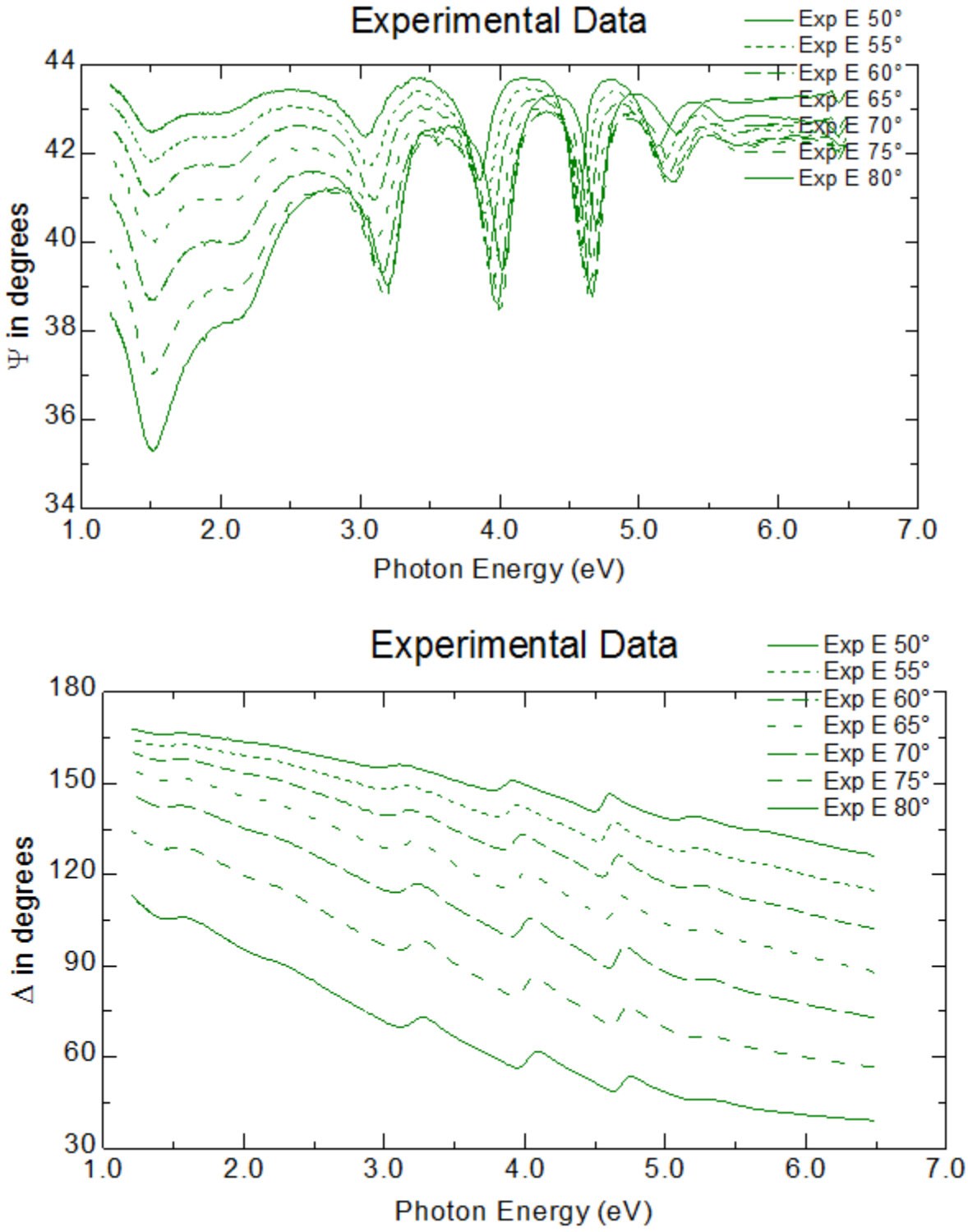

Figure 5: Graphs of ψ vs. photon energy and Δ vs. photon energy for ellipsometric data collected 0.58 hours after sample was exposed to atmosphere at incident angles between 50° and 80°. Exp E denotes ellipsometric reflection data rather than transmission data.

2.2.b SEM

To confirm our ellipsometric analysis of deposited aluminum fluoride thickness, we performed scanning electron microscope (SEM) energy dispersive x-ray (EDX) analysis at 3kV for 100 seconds over an area of 649 µm x 500 µm (Fig. 6).

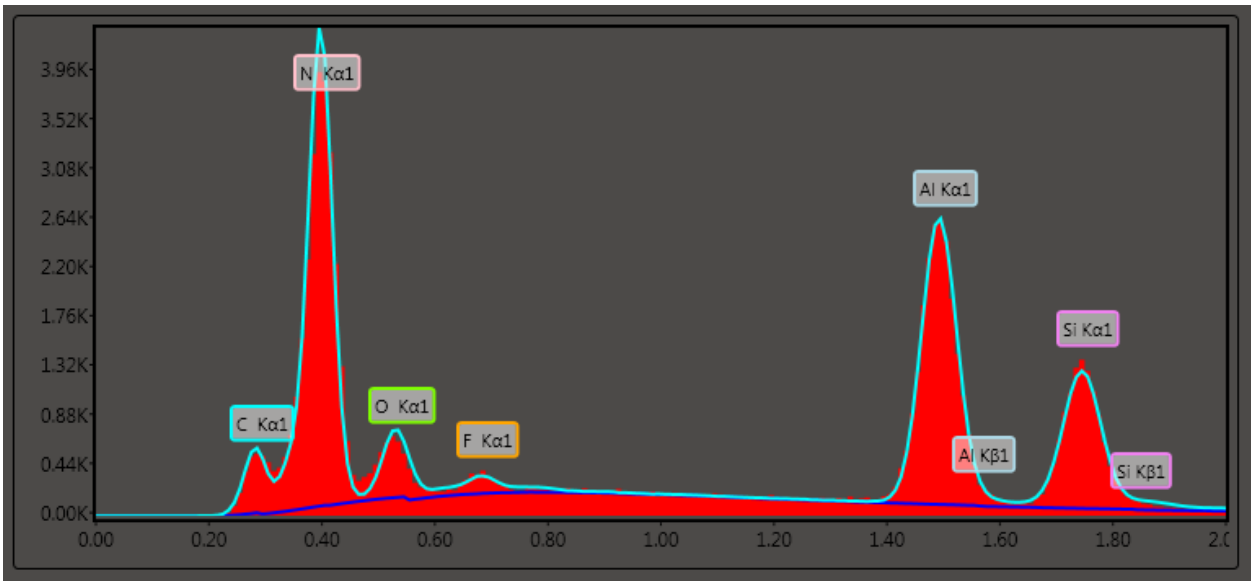

Figure 6: SEM EDX microanalysis element identification spectrum for sample with about 22 nm of Al and 2.4 nm of AlF_3.

2.2.c AFM

Consideration of surface roughness is essential for materials developed for telescope mirrors. Increased surface roughness increases scattering which decreases reflected radiation detected by the telescope. Since the roughness of the aluminum fluoride coating could significantly impact mirror reflectance, we used a Dimension 3100 atomic force microscope (AFM) with a silicon tip in tapping mode over an area of 10 µm x 10 µm to determine surface root mean square (rms) roughness of the AlF_3. Analysis of the surface using AFM was performed at four different locations across the sample to determine average roughness. Initial observation of the AFM images showed a fairly uniform surface with small features (Fig. 7).

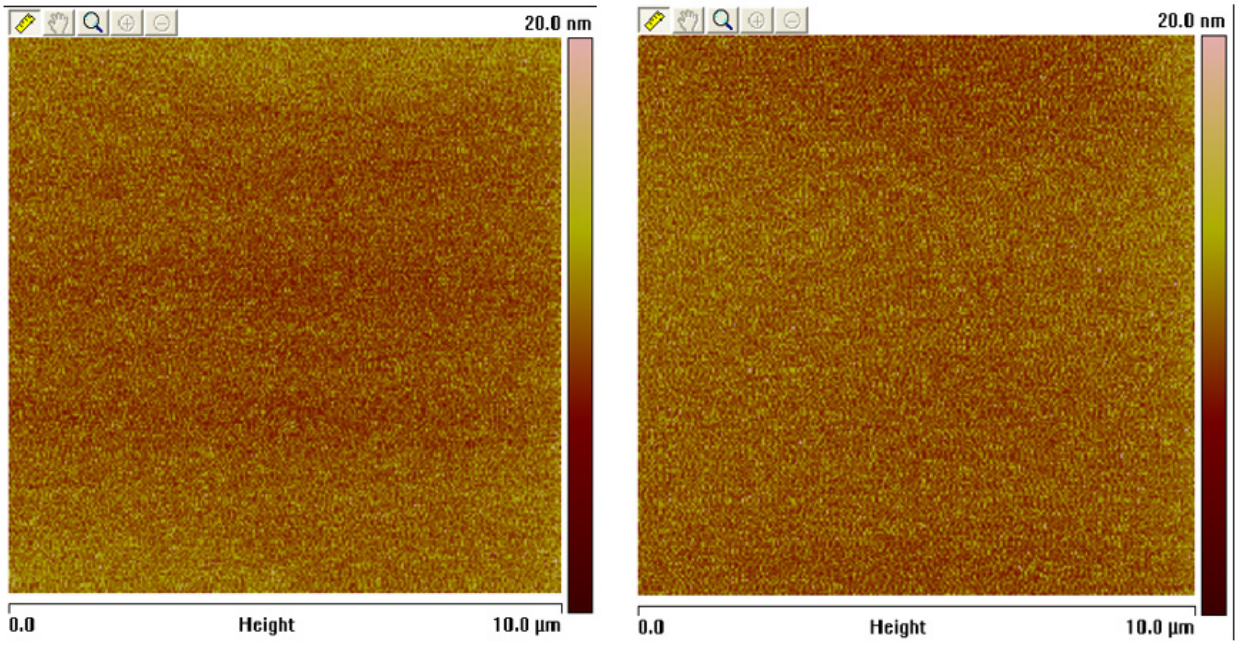

Figure 7: AFM images of AlF_3 surface at two of the locations analyzed.

Chapter 3: Analysis

3.1 Ellipsometry Analysis

Spectroscopic ellipsometric data was processed using WVASE software.[19] The model used for fitting data (Fig. 8) consisted of a silicon (Si) substrate with surface oxide (SiO_2), a silicon nitride (Si_3N_4) layer, deposited aluminum (Al), aluminum oxide (Al_2O_3) growth, deposited aluminum fluoride (AlF_3), and surface roughness. The silicon oxide layer was modeled as two layers: an interface layer and a silicon oxide layer because adding an interface layer is known to substantially improve the data fit.[20] The presence of the silicon nitride layer enhanced our ability to determine layer thicknesses since its interference fringes shifted due to films deposited on top of it.[21]

layer #	type of layer
8	surface roughness
7	AlF_3
6	Al_2O_3
5	Al
4	Si_3N_4
3	SiO_2
2	interface
1	Si

Figure 8: Layer model used for fitting ellipsometric data.

The WVASE software allowed fitting of the optical constants for each layer as well as the thickness of the layer. Thicknesses and optical constants for Si, the interface layer, and SiO_2 were fixed during all fits (Fig. 9).

layer	method of determining thickness (thickness)	method of determining optical constants	model used to determine optical constants
surface roughness	ellipsometry (0 nm)		
AlF_3	ellipsometry (2.4 nm)	ellipsometry of data sets with little Al_2O_3	Cauchy model
Al_2O_3	ellipsometry (varied)	ellipsometry of data sets with thicker Al_2O_3 layers	Cauchy model with Urbach tail
Al	ellipsometry (varied)	ellipsometry	Palik model: Drude component + 2 oscillators
Si_3N_4	ellipsometry (varied)	ellipsometry before deposition	parametric oscillator model
SiO_2	used typical thickness (2.0 nm)	constants provided by J.A. Woollam[22]	
interface	used typical thickness (0.5 nm)	constants provided by J.A. Woollam	
Si	infinitely thick for ellipsometric purposes	constants provided by J.A. Woollam	

Figure 9: Methodology for determination of thicknesses and optical constants for sample layers. Entries in green were fit in preliminary analyses. Entries in blue were fit in the final analysis.

Optical constants for Si_3N_4, Al, AlF_3, and Al_2O_3 as well as surface roughness and thicknesses of AlF_3 and Si_3N_4 were fit in preliminary analyses. Preliminary fitting revealed a variation in Si_3N_4 thickness over the data sets. Since data was taken at slightly different locations on the sample over time, it was reasonable to assume that the Si_3N_4 thicknesses actually differed. For this reason, we allowed the Si_3N_4 thickness to vary in the final fitting. Preliminary fits converged with minimal error when surface roughness was 0 ± 0.04 nm. Therefore, we fixed roughness at 0 nm for the final analysis.

It is generally difficult to separate two dielectric thin film layers (such as AlF_3 and Al_2O_3) using ellipsometry, so we needed to accurately determine the thickness of the AlF_3 layer and fix it during the final fitting. We were able to differentiate between the layers because AlF_3 has little absorption and low dispersion over these photon energies while Al_2O_3 has high dispersion and becomes absorbing above 5.5 eV. We found the AlF_3 thickness to be 2.43 ± 0.1 nm.

Once we had fixed the optical constants for all layers, we simultaneously fit all data sets for our sample (Fig. 10). This fit determined the thicknesses of aluminum, aluminum oxide, and silicon nitride (Fig. 11,12).

layer #	type of layer	thickness of layer
8	surface roughness	0.000 nm
7	AlF_3	2.4 nm
6	Al_2O_3	0.077 nm
5	Al	21.792 nm
4	Si_3N_4	293.074 nm
3	SiO_2	2.000 nm
2	interface	0.500 nm
1	Si	9999990.00 nm

Figure 10: Model used to simultaneously fit all ellipsometry data for our sample using WVASE software. Values in blue were allowed to vary during the fit. Values in black were fixed.

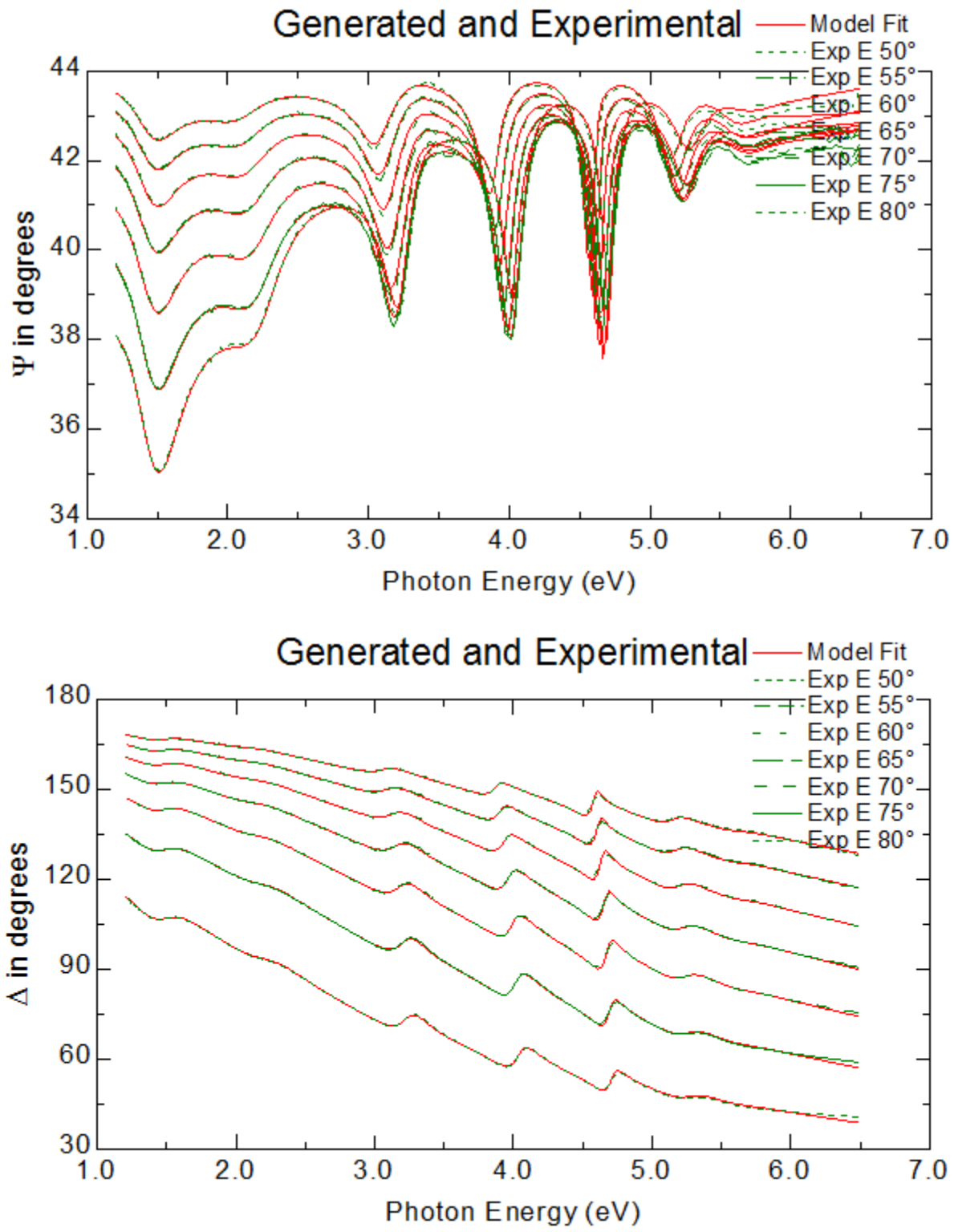

Figure 11: Data and fit for ψ vs. photon energy and Δ vs. photon energy for ellipsometric data collected 0.58 hours after sample was exposed to atmosphere. Exp E denotes ellipsometric reflection data rather than transmission data. As shown in the legend, green lines are data and red are data fit lines.

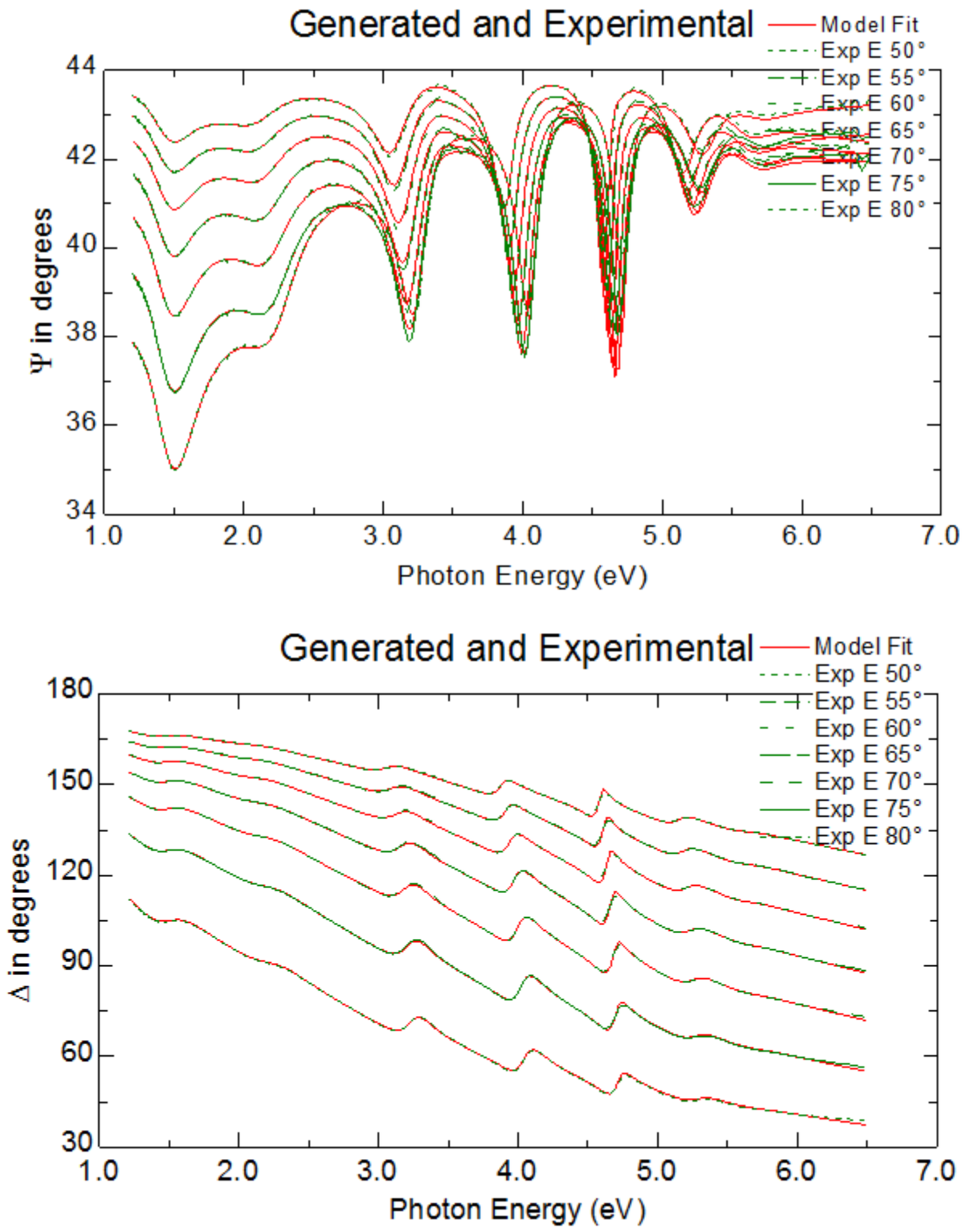

Figure 12: Data and fit for ψ vs. photon energy and Δ vs. photon energy for ellipsometric data collected 116 hours after sample was exposed to atmosphere. Exp E denotes ellipsometric reflection data rather than transmission data. As shown in the legend, green lines are data and red are data fit lines.

These fits allowed the determination of the thicknesses of aluminum and aluminum oxide as well as the thickness of the silicon nitride layer. As shown in Table 1, Al_2O_3 thickness increased over time while Al and Si_3N_4 thicknesses varied slightly. Errors given for the ellipsometric fits were significantly smaller than the thicknesses given.

time (hours)	Al_2O_3 thickness (nm)	Al thickness (nm)	Si_3N_4 thickness (nm)
0.58	0.077±0.00205	21.792±0.00870	293.074±0.0251
1.37	0.249±0.00243	22.276±0.01090	291.933±0.0308
2.55	0.190±0.00186	21.509±0.00724	293.042±0.0244
4.00	0.284±0.00195	21.589±0.00769	292.201±0.0259
8.25	0.404±0.00197	21.785±0.00824	293.139±0.0255
22.88	0.573±0.00207	21.754±0.00855	293.526±0.0261
30.00	0.586±0.00195	21.542±0.00780	292.323±0.0246
48.60	0.890±0.00191	21.738±0.00747	291.658±0.0259
76.90	0.763±0.00183	21.531±0.00704	292.265±0.0245
102.20	0.800±0.00197	22.336±0.00882	293.611±0.0270
116.00	0.902±0.00199	20.958±0.00731	292.290±0.0232

Table 1: Thicknesses extracted from all data sets with errors given by the WVASE software.

3.2 Statistical Analysis

Plotting silicon nitride thickness as a function of oxidation time (Fig. 13) showed a maximum 2 nm variation in thickness. Since the error in the ellipsometric fit (error bars shown) was much smaller than the residual, changes in the Si_3N_4 thickness over time were not likely due to error in the fit. Rather, the variations in thickness were likely caused by systematic error such as

fluctuations in Si_3N_4 thickness across the sample. Fitting the Si_3N_4 thickness gave the linear model

$$Si_3N_4\ thickness = (292.653 \pm 0.285) - (0.000295 \pm 0.00516)\ time$$

where thickness was in nanometers and time was in hours.

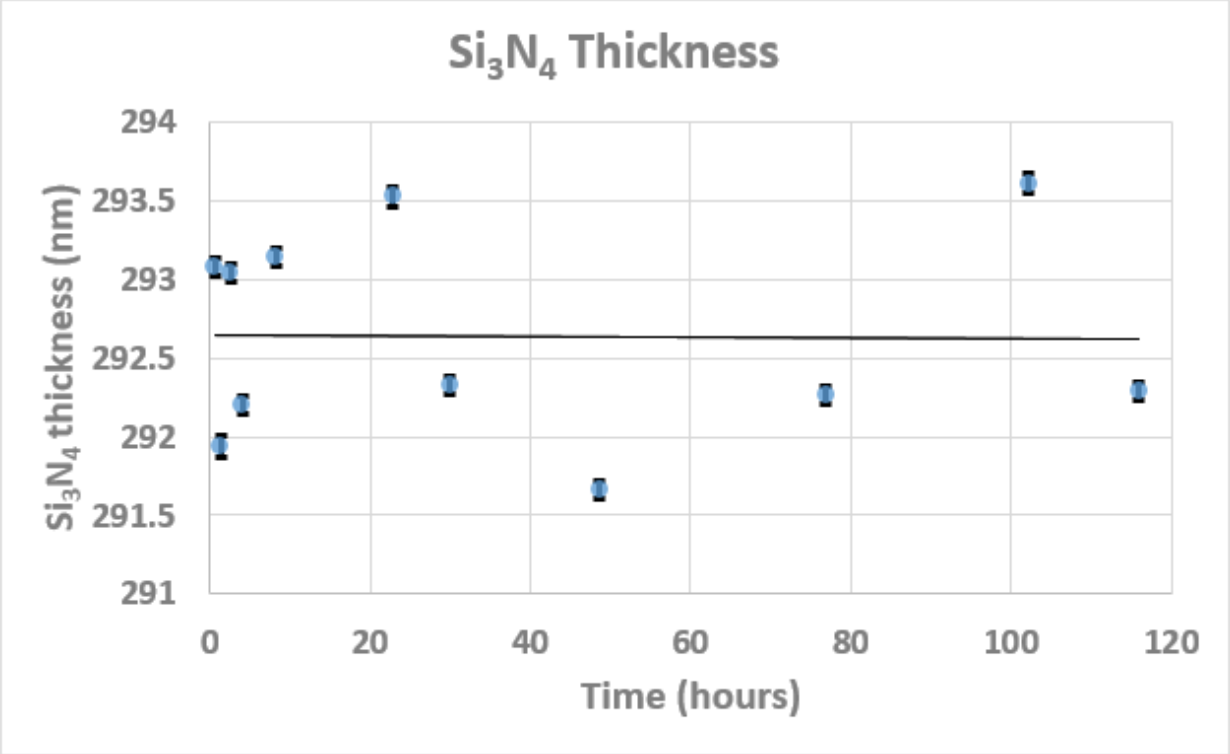

Figure 13: Linear fit of Si_3N_4 thickness as a function of oxidation time.

Although the negative slope in the fit could have suggested a decrease in Si_3N_4 thickness over time, the uncertainty in the slope was larger than the slope value – so the slope was not statistically significant. Therefore, the linear fit showed no relationship between Si_3N_4 thickness and oxidation time. Since ellipsometric measurements were taken at slightly different locations on the sample, it was reasonable to conclude that Si_3N_4 thickness varied across the sample surface but did not vary as a function of time.

Plotting aluminum thickness versus oxidation time (Fig. 14) showed very little error in the ellipsometric fit (error bars shown). Fitting the Al data showed the Al thickness over time to be modelled by:

$$Al\ thickness = (21.850 \pm 0.204) - (0.0544 \pm 0.0655)\ \ln(time)$$

with thickness in nanometers and time in hours.

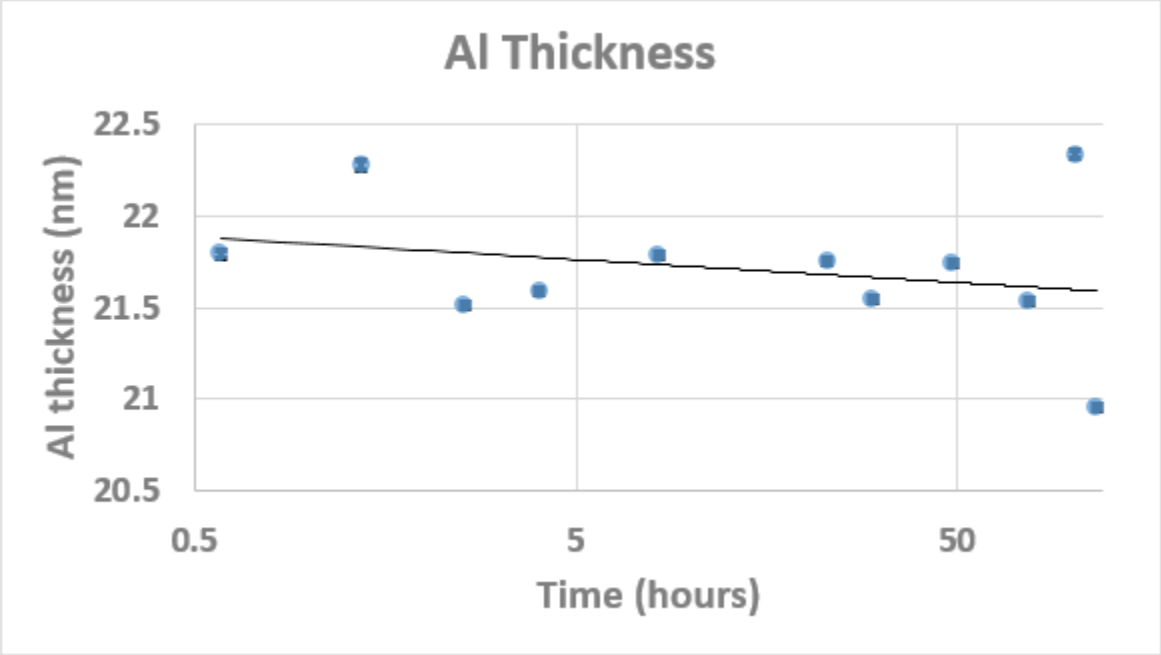

Figure 14: Logarithmic fit of Al thickness as a function of oxidation time.

We expected the fit to show a decrease in Al thickness as a function of time – corresponding physically to a decrease in Al thickness as Al oxidized and the Al_2O_3 layer grew – and fitting this data showed that decrease. However, the error in the slope of the fit line is larger than the slope itself – which might render the decrease in Al thickness statistically insignificant. Additionally, we knew how much the Al_2O_3 thickness grew – so we knew how much the Al thickness should decrease. Since Al density in Al_2O_3 is less than in Al, we expected the decrease in thickness of Al to be less than the increase in thickness of Al_2O_3. Specifically, the density of Al atoms is 6.02×10^{22} atoms/cm^3 and the density of Al_2O_3 molecules is 2.34×10^{22} molecules/cm^3 with 2 Al

atoms in each Al_2O_3 molecule, so we expected the Al layer to decrease over the entire oxidation time by $\frac{2\ (2.34\ x\ 10^{22})}{6.02\ x\ 10^{22}}$ or 0.78 times the increase in thickness of Al_2O_3. This predicted a decrease in Al thickness of 0.644 nm, but the fit function for our Al data only shows a decrease of 0.258 nm. This disparity could be explained by the fact that 0.644 nm is relatively small compared to the overall Al thickness of 21.850 nm – so it would have been difficult for the ellipsometry software to accurately fit the change in thickness. However, using the 95% confidence limit yielded slope values for the Al data fit between -0.185 nm/hr and 0.077 nm/hr which gave changes in Al thickness between -0.880 nm and 0.364 nm. The expected decrease, -0.644 nm, fell within that range. So the amount of decrease in Al thickness that corresponds to the growth in Al_2O_3 thickness is within the 95% confidence limit of the fit for our data.

Plotting aluminum oxide thickness over time (Fig. 15) showed a clear increase in Al_2O_3 as a function of time. The data trend was logarithmic, which is what we expected for oxidation: as oxygen first contacted the aluminum, the oxidation reaction could easily occur; however, as the aluminum oxide began to grown on the aluminum surface, oxygen had to penetrate below the top oxide layers for further oxidation of aluminum to happen. This caused a decrease in the oxidation rate.

The small size of the error bars compared to the overall change in Al_2O_3 thickness suggested that thicknesses determined from the ellipsometric fit were very accurate.

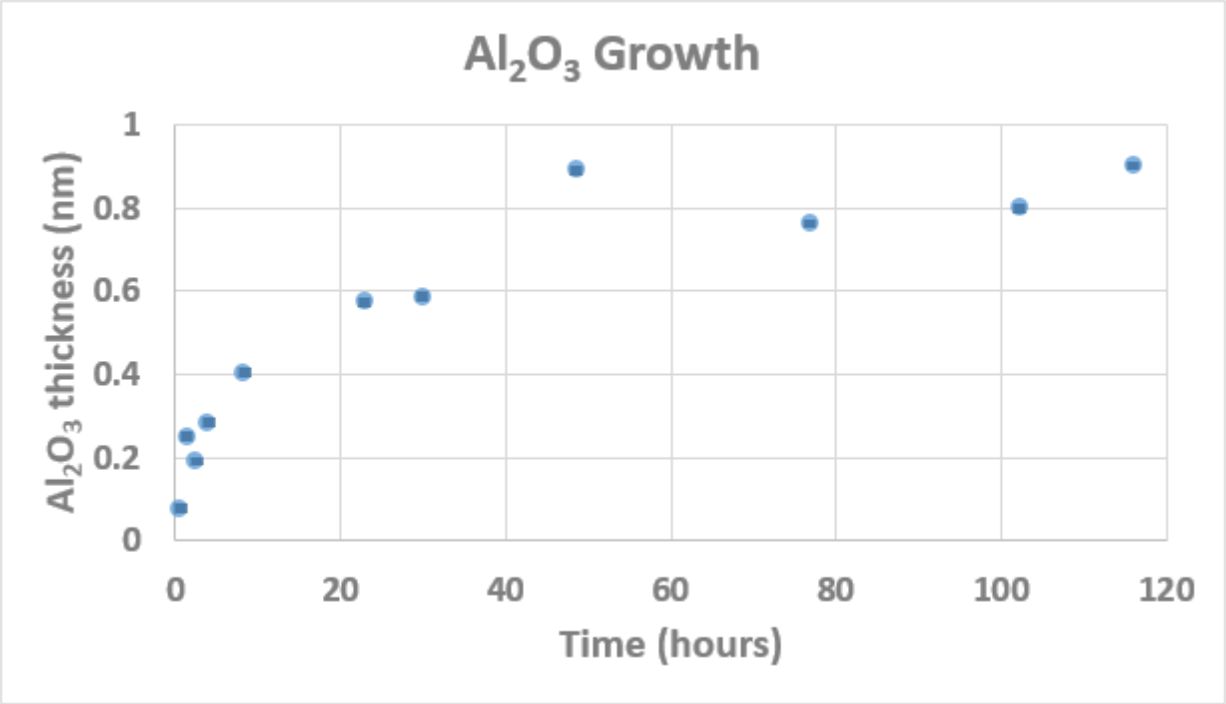

Figure 15: Derived Al_2O_3 thickness as a function of oxidation time.

Fitting the Al_2O_3 data (Fig. 16) showed the Al_2O_3 growth to be modelled by:

$$Al_2O_3 thickness = (0.120 \pm 0.0401) + (0.155 \pm 0.0129)\ \ln(time)$$

with time in hours and thickness in nanometers.

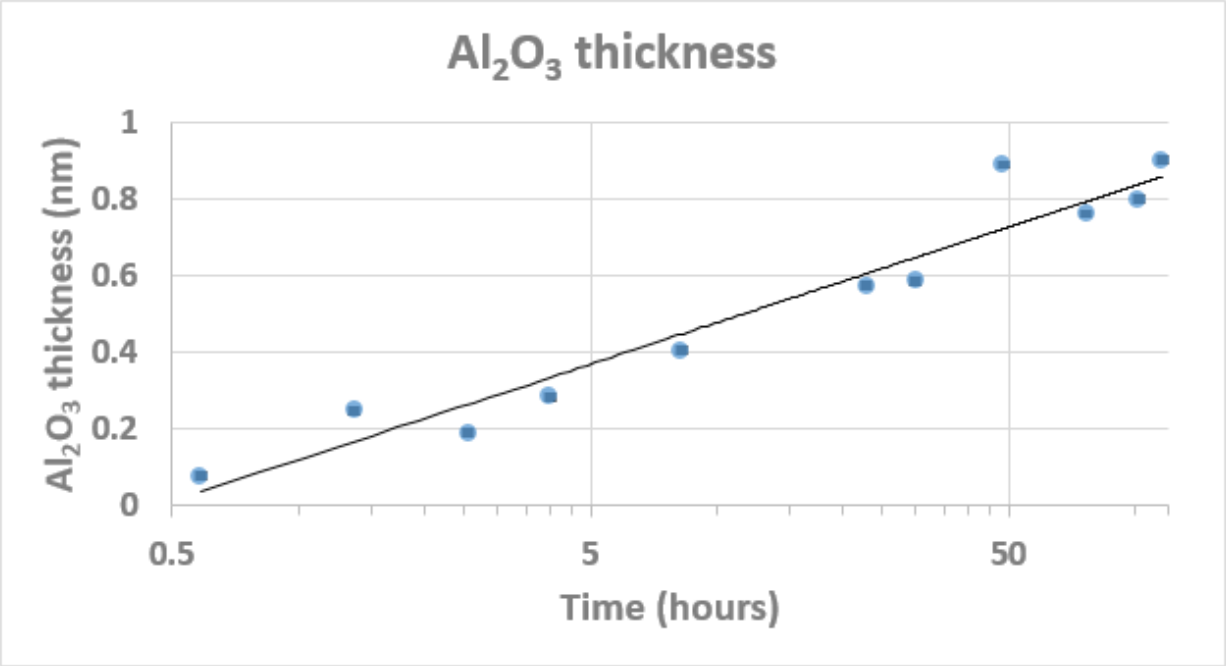

Figure 16: Relationship of Al_2O_3 growth to oxidation time.

Small uncertainties in the fit equation parameters relative to the parameters themselves demonstrated that our growth rate equation modelled the physical aluminum oxide growth very well.

3.3 SEM Analysis

We performed SEM EDX analysis to confirm the thicknesses resulting from ellipsometry data fitting. Since EDX spectra only show relative amounts of elements, we first analyzed a sample with approximately 30 nm of aluminum and 28 nm of aluminum fluoride. We compared that sample's spectrum to the spectrum from the sample we performed ellipsometry on (with approximately 22 nm of aluminum and 2.4 nm of aluminum fluoride) (Fig. 17).

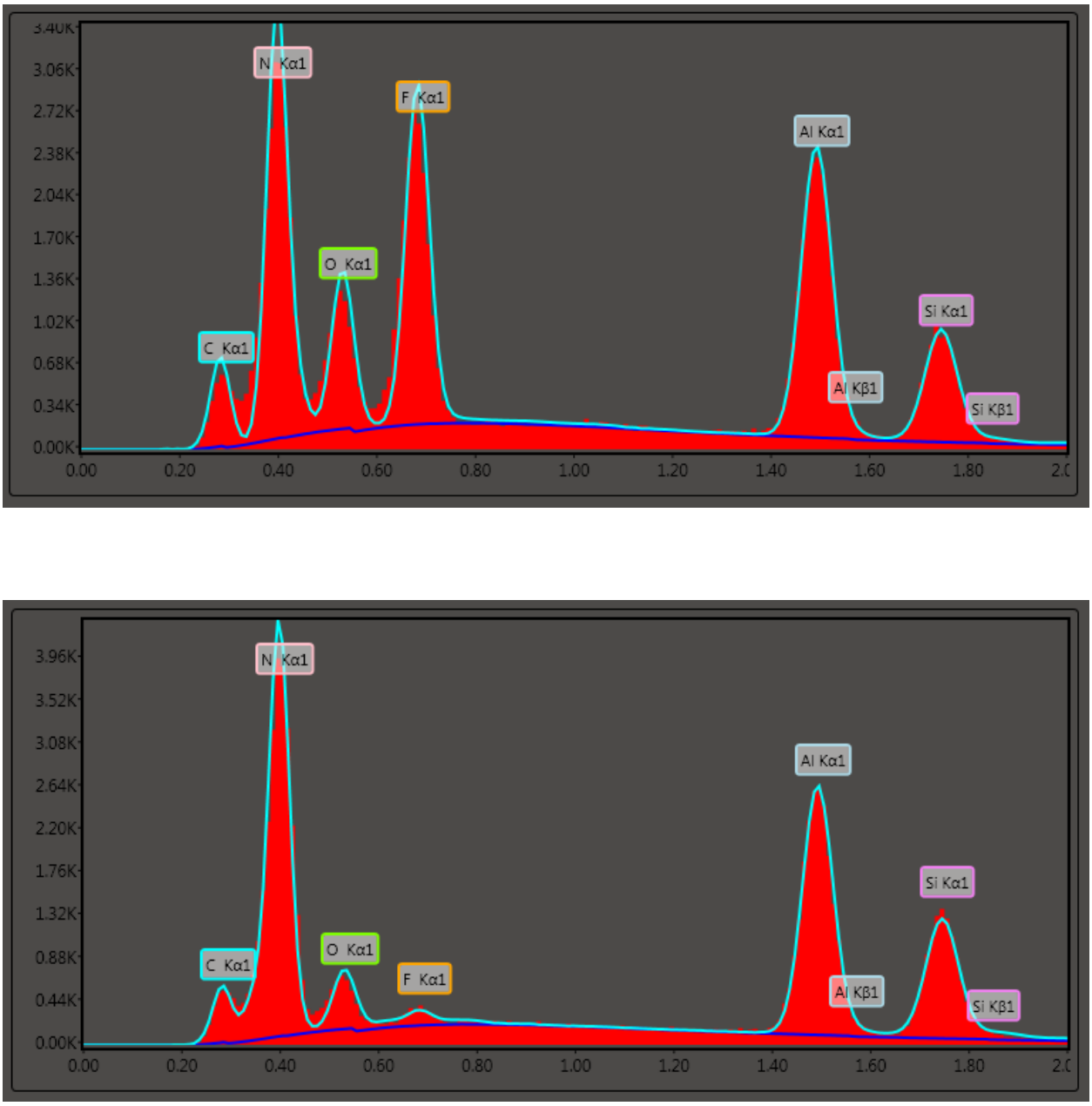

Figure 17: SEM EDX microanalysis element identification spectra for comparison sample with approximately 30 nm Al and 28 nm AlF_3 which oxidized 241 hours (top) and analyzed sample with approximately 22 nm Al and 2.4 nm AlF_3 after oxidizing 97 hours (bottom).

The spectra confirmed the presence of aluminum and fluorine on both samples. The ratio of fluorine to silicon on the comparison sample was significantly higher than the same ratio on the sample in question. This suggests that the AlF_3 layer on our sample was significantly thinner

than 28 nm. Indeed, the 2.4 ± 0.1 nm ellipsometric fit may be accurate. The oxygen to silicon ratio was also larger on the comparison sample. This could be due to aluminum oxide growth since the comparison sample was exposed to atmosphere for 144 hours longer than the sample analyzed by ellipsometry. The increase in oxygen could also be accounted for by the thicker Al and AlF_3 layers in the comparison sample: since pressure in the deposition chamber rose considerably during deposition, it's likely that the Al and AlF_3 layers contain some oxygen. Since our deposition system was an oil diffusion pump system, we examined the SEM spectrum for evidence of hydrocarbons in our sample. Hydrogen can't be identified using EDX analysis, but our spectra did show distinct carbon peaks. This could be evidence of hydrocarbons in our deposition system, but carbon is generally deposited on samples by the microscope beam during EDX analysis so the presence of carbon in the spectrum isn't conclusive proof of hydrocarbons. Additionally, our deposition system includes a liquid nitrogen cold trap to prevent the escape of hydrocarbons from the pump into the vacuum chamber and samples deposited in this system haven't historically shown evidence of the incorporation of hydrocarbons. Therefore, the EDX analysis didn't raise serious concerns about the presence of hydrocarbons in the sample.

3.4 AFM Analysis

Our ellipsometric data fitting determined surface roughness to be 0 ± 0.04 nm. To confirm this value we also used atomic force microscopy (AFM) characterization of the surface. Root mean square roughness of the sample surface – as determined by AFM at four locations across the sample surface – was 0.325-1.15 nm. Pictures of the surface (Fig. 18) showed a fairly uniform surface with small features over a 10 μm x 10 μm area.

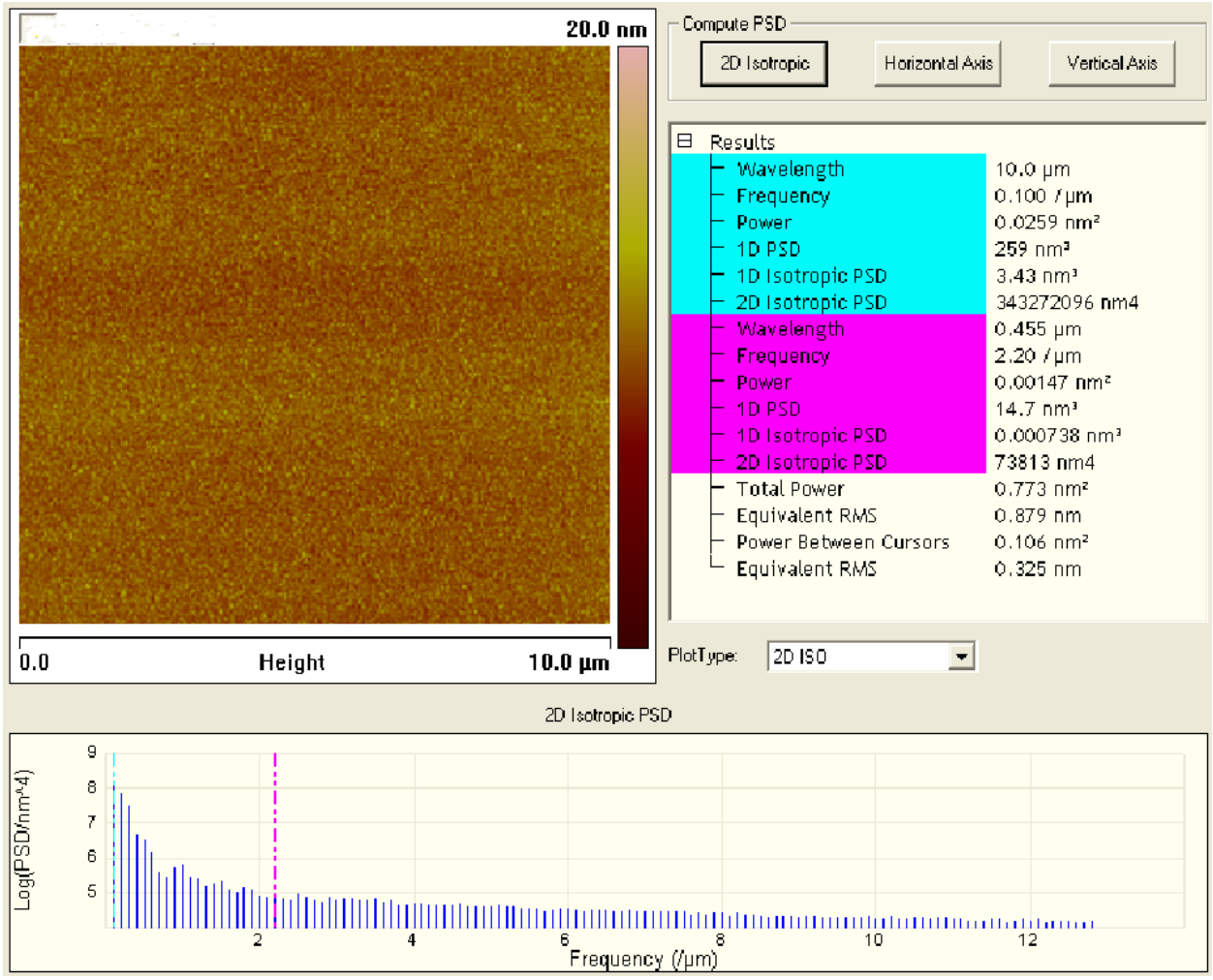

Figure 18: AFM image of AlF_3 surface (top left) with power spectral density graph (bottom). Calculated rms roughness for this location on the sample is shown at right.

The power spectral density graph (Fig. 15) shows that the roughness density distribution is higher at lower spatial frequencies. The characteristic length scale of the roughness is longer than 2 µm. This could explain why we didn't see roughness in the ellipsometry fit since the ellipsometer wouldn't be as sensitive to these lower spatial frequencies.

Chapter 4: Discussion and Conclusion

4.1 Discussion

4.1.a Experimentally-Determined Optical Constants

Optical constants for Si_3N_4, Al, and AlF_3 determined by ellipsometric fitting were very similar to literature optical constants[12] for those materials (Fig. 19-21). Optical constants for Al_2O_3 showed a slight difference between literature and experimental n values, but thickness determination was not sensitive to that amount of change in n: either set of values for n produced essentially the same layer thicknesses. The optical constants for aluminum oxide growing on our sample showed our oxide to be more absorbing at high energies than literature Al_2O_3 (Fig. 22). This was to be expected since literature optical constants for Al_2O_3 assume single crystal sapphire while our oxide formed at room temperature and its structure was likely more disordered.

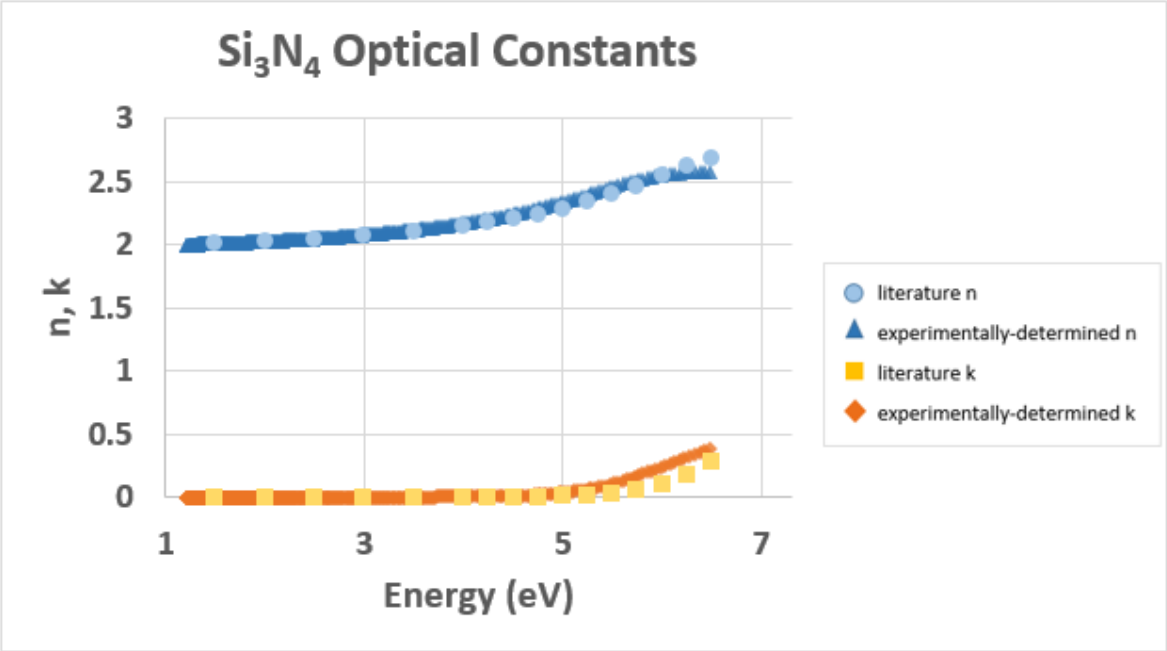

Figure 19: Optical constants for Si_3N_4 as determined by ellipsometric fitting as compared to optical constants from literature[12]. n and k are the components of the complex index of refraction where index = n + *i* k.

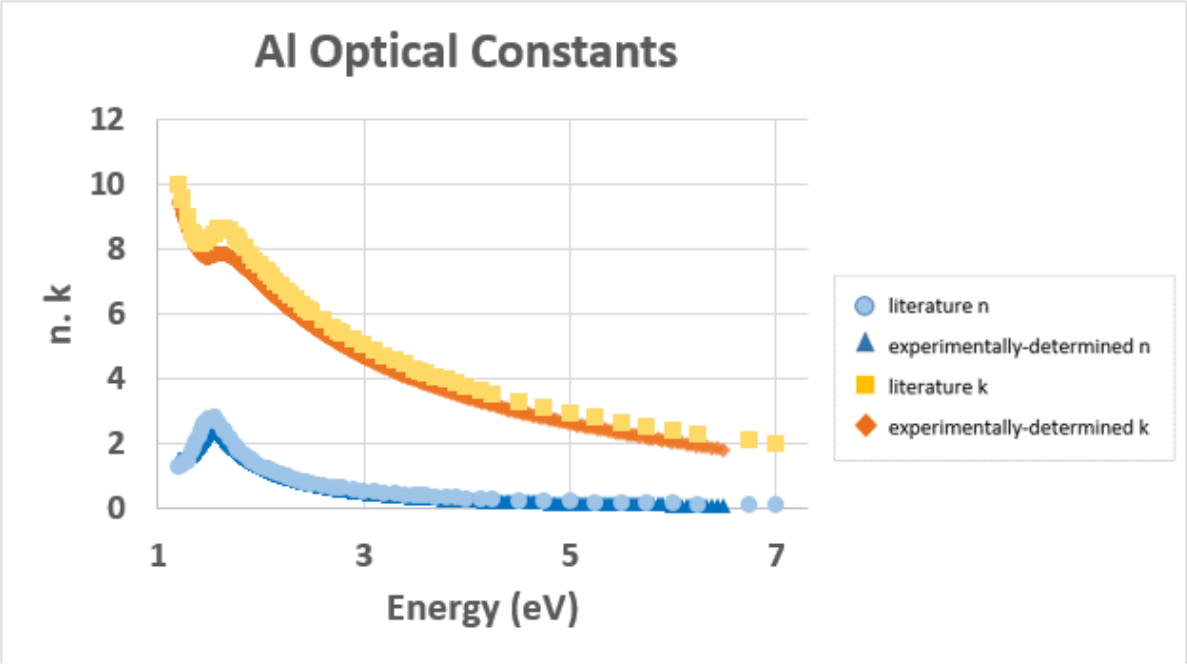

Figure 20: Optical constants for Al as determined by ellipsometric fitting as compared to optical constants from literature[12]. n and k are the components of the complex index of refraction where index = n + *i* k.

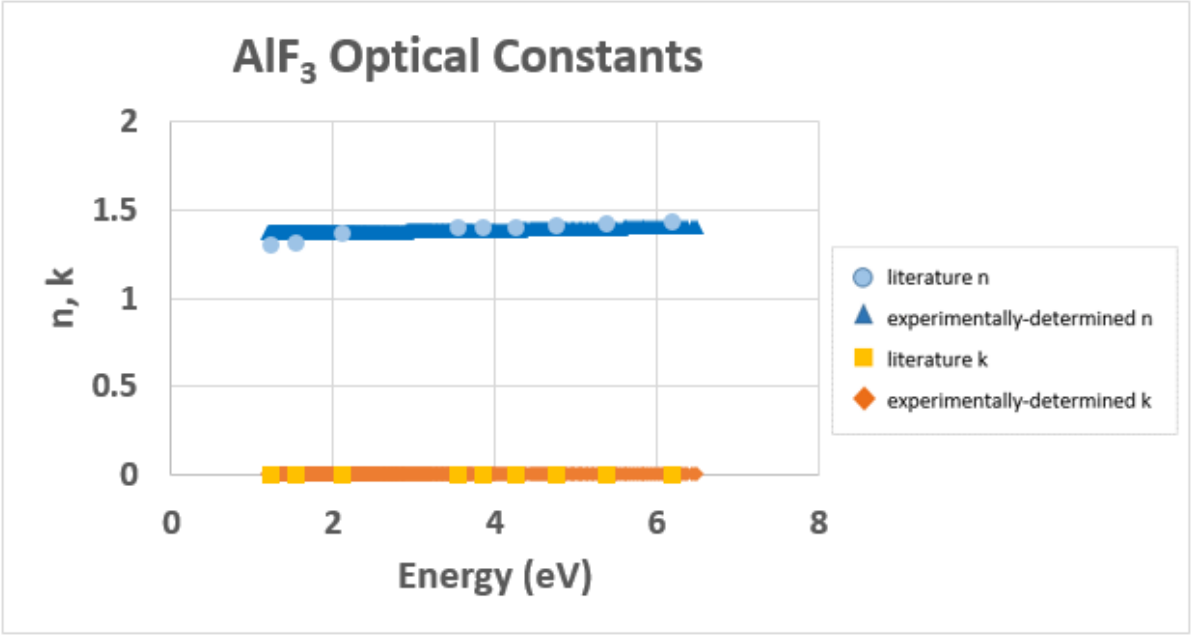

Figure 21: Optical constants for AlF_3 as determined by ellipsometric fitting as compared to optical constants from literature[12]. n and k are the components of the complex index of refraction where index = n + *i* k.

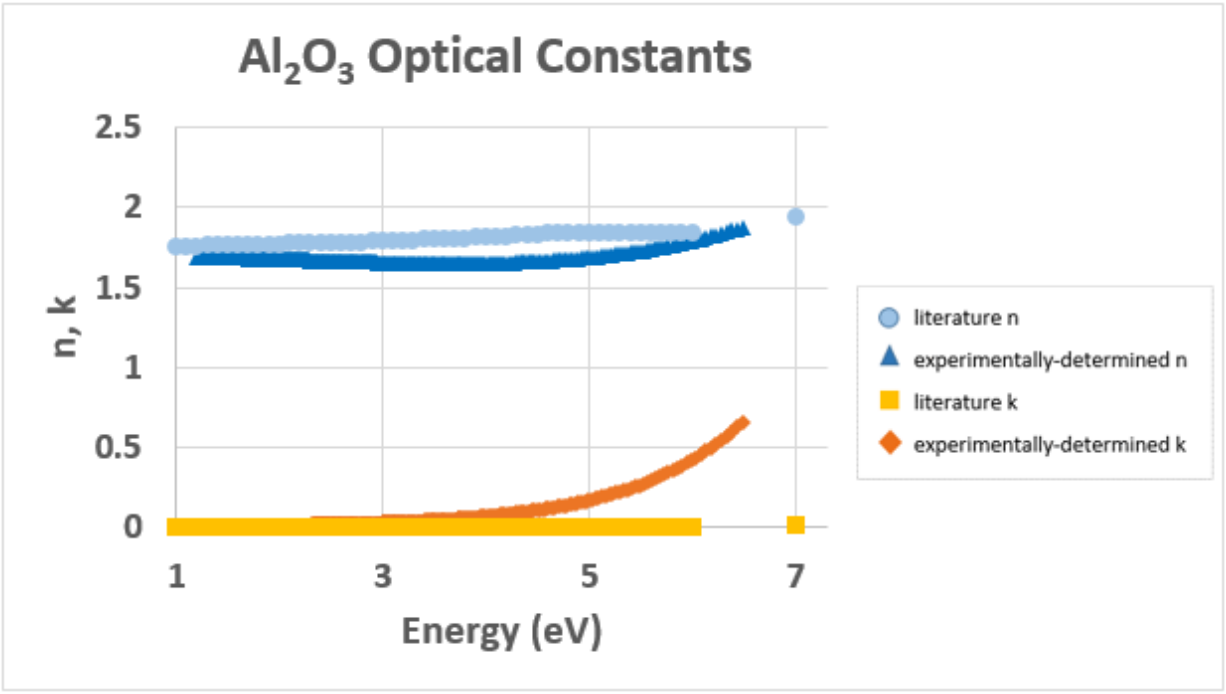

Figure 22: Optical constants for Al_2O_3 as determined by ellipsometric fitting as compared to optical constants from literature[12]. n and k are the components of the complex index of refraction where index = n + *i* k.

4.1.b Retarding of Aluminum Oxide Growth

To determine how well AlF_3 protected aluminum against oxidation, we compared our Al_2O_3 growth to Al_2O_3 growth on bare Al. We used data from R. P. Madden et al.[11,22] as our comparison. Madden evaporated Al in vacuum, measured reflectance over time while the Al was still in vacuum (5 x 10^{-7} torr), exposed the sample to air, and then measured reflectance over time while the sample was in air. We used Madden's reflectance data along with theoretical reflectance data for Al with Al_2O_3 growth to determine the growth of Al_2O_3 on bare Al over time. For the bare Al in vacuum, approximately 0.75 nm of Al_2O_3 grew on the sample surface in 0.67 hours. By comparison, for the AlF_3-protected Al sample in air, less than 0.1 nm of Al_2O_3 grew on the sample surface in the same amount of time (Fig. 23). This showed that using a layer of AlF_3 to retard oxidation of Al was even more effective than keeping the Al in vacuum.

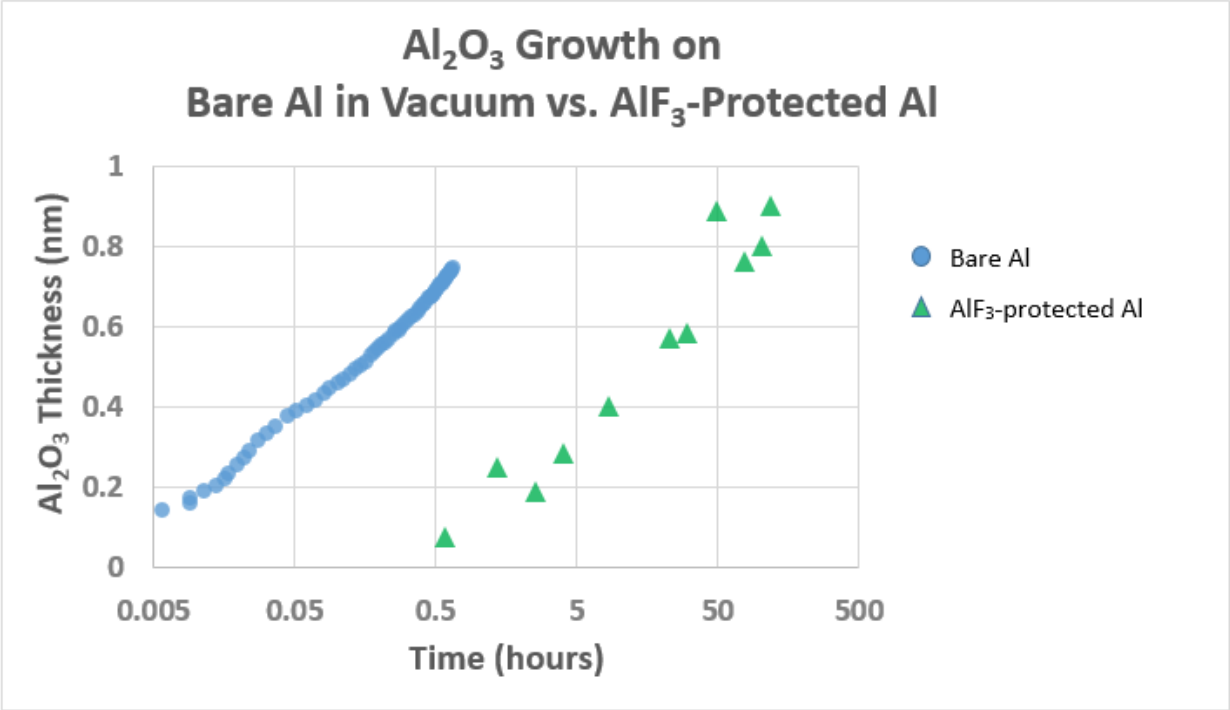

Figure 23: Al_2O_3 growth on bare Al in vacuum at 5 x 10^{-7} torr (Madden[11] data) vs. AlF_3-protected Al in air (our data).

For the bare Al sample kept in vacuum for eight minutes and then exposed to air, more than 1 nm of Al_2O_3 grew on the sample surface in less than 1 hour. In contrast, the AlF_3-protected sample had an Al_2O_3 thickness less than 1 nm over a period of 116 hours (Fig. 24). Clearly, the AlF_3 layer was effective in retarding oxidation of aluminum.

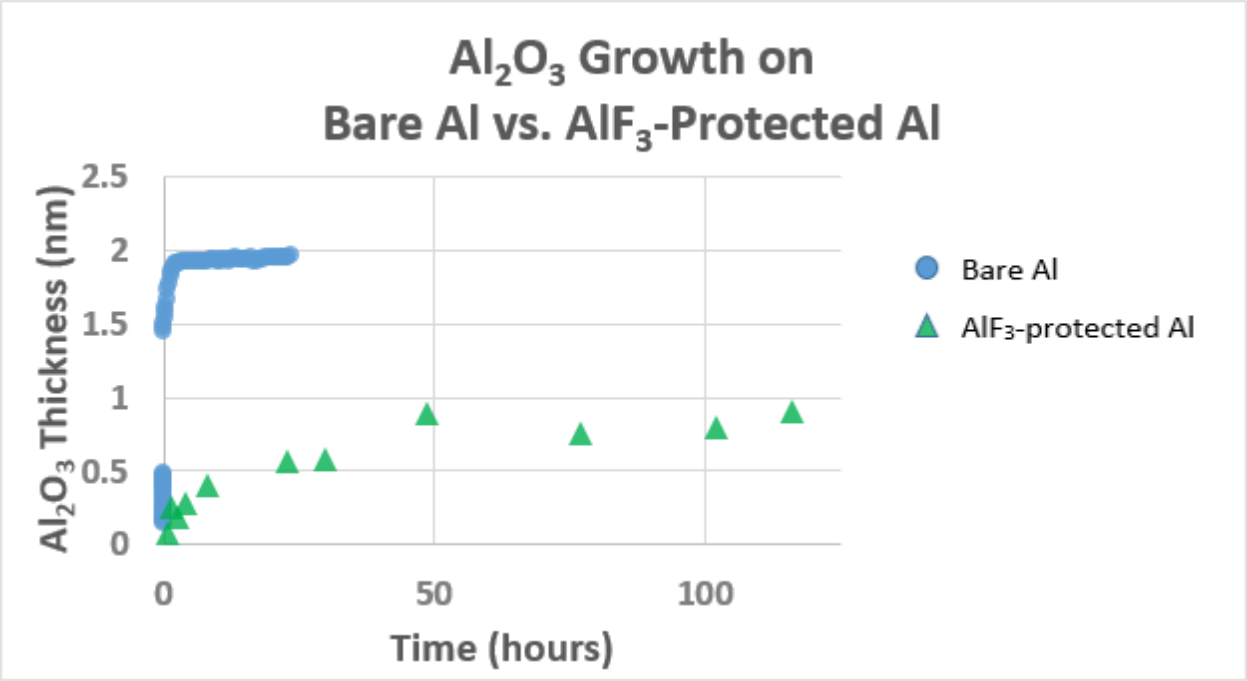

Figure 24: Al_2O_3 growth on bare Al kept 8 minutes in vacuum and then 24 hours in air (Madden[11] data) vs. AlF_3-protected Al in air (our data). Split in bare Al graph shows rapid initial oxidation of Al upon exposure to air.

4.1.c Preservation of Aluminum's Reflectance in the Ultraviolet

Our data unquestionably showed that AlF_3 impeded the growth of Al_2O_3 on an Al mirror. The reason we wanted to impede oxide growth was to preserve aluminum's high reflectance in the ultraviolet. For this reason, we compared the reflectance of AlF_3 on Al to the reflectance of Al_2O_3 on Al to be sure that AlF_3 preserved aluminum's ability to reflect well in the ultraviolet (Fig. 25). Since Madden's data showed 2 nm of Al_2O_3 forming on bare Al, we used that thickness in our comparison. It was clear that AlF_3 allowed much higher Al reflectance than

2 nm Al_2O_3 over the ultraviolet wavelength range. Therefore, the AlF_3 coating would allow the reflectance of those key ultraviolet spectral lines of interest to astrophysicists.

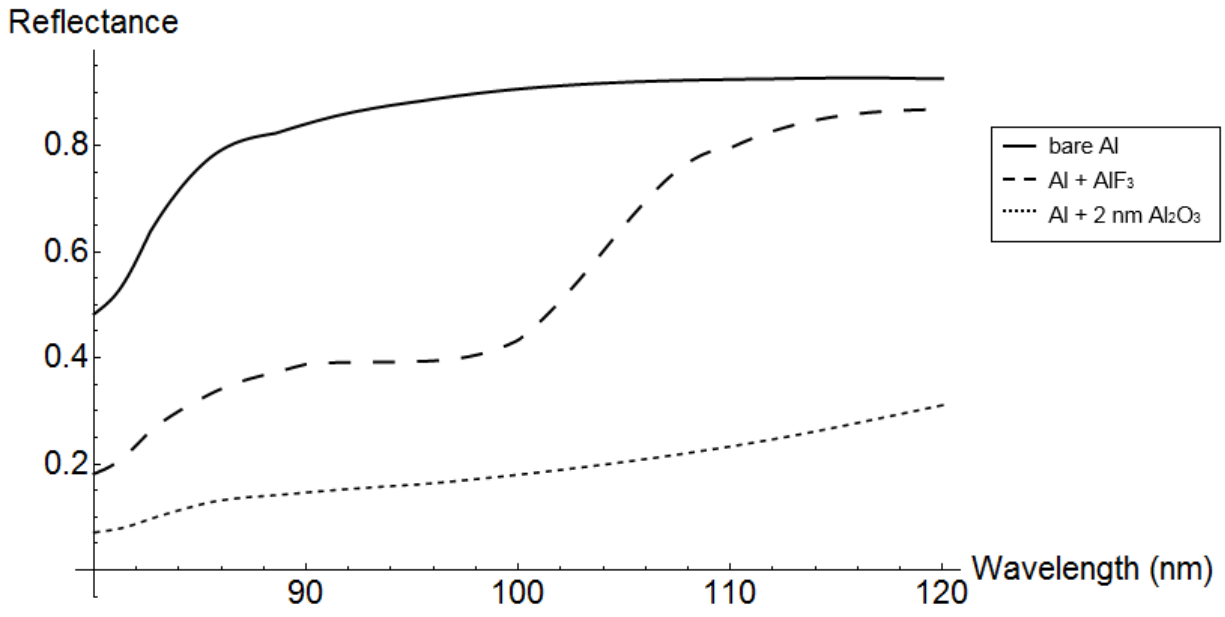

Figure 25: Reflectance in the ultraviolet of AlF_3-protected Al compared to Al with 2 nm Al_2O_3 growth. Reflectances were calculated using the Parratt method employing literature optical constants[12].

4.1.d Surface Roughness

We initially determined surface roughness during preliminary ellipsometric fits (Table 2). Although a few roughness values determined in this manner were greater than 0 nm, the amount of error associated with those values suggested that it was reasonable to set roughness at 0 nm over the entire oxidation time. Fitting Al_2O_3 thickness using a surface roughness of 0 nm as opposed to fitting the thickness while allowing roughness to vary as shown in Table 2 yielded nearly identical values for Al_2O_3 layer thicknesses over time.

time (hours)	roughness (nm)
0.58	0.000 ± 0.0382
1.37	0.000 ± 0.0423
2.55	0.000 ± 0.0370
4.00	0.000 ± 0.0386
8.25	0.000 ± 0.0380
30.00	0.000 ± 0.0378
48.60	0.001 ± 0.0375
76.90	0.001 ± 0.0369
102.20	0.052 ± 0.0378
116.00	0.017 ± 0.0381

Table 2: Surface roughness as determined by ellipsometric fitting. Mean square error (MSE) associated with this fit was 5.002.

Since later AFM characterization of the sample surface yielded rms roughnesses between 0.325 nm and 1.15 nm, we repeated our ellipsometric fit – using these new values for surface roughness. Fits using different surface roughnesses produced different values for Al_2O_3 thickness over time (Table 3).

time (hours)	Al_2O_3 thickness (nm)		
	roughness set at 0 nm	roughness set at 0.325 nm	roughness set at 1.15 nm
	MSE = 5.025	MSE = 5.195	MSE = 10.27
0.58	0.077 ± 0.00205	0.000 ± 0.00212	0.000 ± 0.00423
2.55	0.190 ± 0.00186	0.054 ± 0.00192	0.000 ± 0.00383
4.00	0.284 ± 0.00195	0.148 ± 0.00202	0.000 ± 0.00402
8.25	0.404 ± 0.00197	0.269 ± 0.00204	0.000 ± 0.00404
22.88	0.573 ± 0.00207	0.438 ± 0.00214	0.095 ± 0.00423
30.00	0.586 ± 0.00195	0.451 ± 0.00201	0.107 ± 0.00399
48.60	0.890 ± 0.00191	0.737 ± 0.00193	0.393 ± 0.00383
76.90	0.763 ± 0.00183	0.627 ± 0.00189	0.283 ± 0.00374
102.20	0.800 ± 0.00197	0.665 ± 0.00203	0.321 ± 0.00403
116.00	0.902 ± 0.00199	0.766 ± 0.00206	0.422 ± 0.00407

Table 3: Determination of Al_2O_3 layer thickness using different values for surface roughness.

The amount of mean square error (MSE) for the different fits suggested that roughness between 0 nm and 0.325 nm (MSE ≈ 5) accurately described the sample while roughness as high as 1.15 nm (MSE = 10.27) was physically unlikely over the bulk of the oxidation time. Since AFM characterization was performed when the sample had oxidized for more than 116 hours, it is possible that the Al_2O_3 layer had grown unevenly under the AlF_3 barrier – causing increased surface roughness that showed in the later AFM measurements but not the earlier ellipsometric data sets. Indeed, the surface roughness fit shown in Table 2 corroborated this theory since it showed roughness increasing as a function of oxidation time. It is also possible that handling of the sample over time contributed to increased surface roughness.

Regardless of the cause of increased roughness over time, our data showed that the AlF_3 barrier layer was deposited with a surface roughness between 0 nm and 0.325 nm which categorized evaporated AlF_3 as a suitable mirror material.

4.2 Conclusion

We were able to adequately determine the optical constants for Al_2O_3 grown on aluminum under a layer of AlF_3 in order to determine the Al_2O_3 growth rate for Al coated with 2.4 nm of AlF_3 and exposed to atmosphere. Our results showed that 2.4 nanometers of aluminum fluoride significantly retarded oxide growth on aluminum. Additionally, we showed that AlF_3 allows Al reflectance in the ultraviolet. We further established that the surface roughness of AlF_3 deposited by thermal evaporation in the manner described is small enough to warrant further investigation of AlF_3 as a mirror coating.

Since aluminum fluoride is currently of great interest to researchers working with reflection of aluminum in the ultraviolet wavelength range, we suggest further investigation with varying

thicknesses of AlF_3 as well as multilayer barriers where AlF_3 is coupled with LiF to prevent oxidation of aluminum mirrors.

Bibliography

[1] Larruquert, J., Mendez, J. and Aznarez, J., "Nonoxidized Al-overcoated Ir bilayers with high reflectance in the extreme ultraviolet above 50 nm," *Opt. Eng.* 41(6), 1418-1424 (2002)
[2] Moore, C.S. et al., "Current progress in the characterization of atomic layer deposited AlF_3 for future astronomical ultraviolet mirror coatings," *Proc. SPIE* 9601, 96010X (2015)
[3] Moore, C.S. et al., "Recent developments and results of new ultraviolet reflective mirror coatings," *Proc. SPIE* 9144, 91444H (2014)
[4] "From Cosmic Birth to Living Earth," http://www.hdstvision.org/ (accessed September 2017)
[5] Shustov, B. et al., "WSO-UV progress and expectations," *Astrophysics and Space Science* 354(1), 155-161 (2014)
[6] Heap, S. et al., "Galaxy evolution spectroscopic explorer: scientific rationale," *Proc. SPIE* 9905, 990505 (2016)
[7] "LUVOIR," https://asd.gsfc.nasa.gov/luvoir/media/Flyer_v5.pdf (accessed September 2017)
[8] "Cosmic Origins," https://cor.gsfc.nasa.gov/studies/ (accessed September 2017)
[9] Balasubramanian, K. et al., "Aluminum Mirror Coatings for UVOIR Telescope Optics including the Far UV," *Proc. SPIE* 9602, 96020I (2015)
[10] Wang, B. and Gallais, L. "A theoretical investigation of the laser damage threshold of metal multi-dielectric mirrors for high power ultrashort application," *Optics Express* 21(12), 14698-14711 (2013)
[11] Madden, R.P., Canfield, L.R., and Hass, G., "On the Vacuum-Ultraviolet Reflectance of Evaporated Aluminum before and during Oxidation," *Journal of the Optical Society of America,* 53(5) (1963)
[12] *Handbook of Optical Constants of Solids.* Edited by E. Palik, Academic Press (1998)
[13] Hass, G. and Hunter, W.R., "Calculated Reflectance of Aluminum-Overcoated Iridium in the Vacuum Ultraviolet from 500 A to 2000 A," *Applied Optics*, 6(12), 2097 (1967)
[14].Appenzeller, I., "UV, X-Ray, and Gamma Spectroscopy," in *Introduction to Astronomical Spectroscopy*. Cambridge University Press (2013)
[15] Karim, A., "Thin Film Heater for Removable Volatile Protecting Coatings," *Scientific World Journal* (2013)
[16] Hennessy, J. et al., "Ultraviolet optical properties of aluminum fluoride thin films deposited by atomic layer deposition*," Journal of Vacuum Science & Technology*, 34(1) (2015)
[17] Wang, X.-D. et al., "Design and fabrication of far ultraviolet filters based on pi-multilayer technology in high-k materials," *Scientific Reports*, 5(8503) (2015)
[18] Wilbrandt, S. et al., "Protected and enhanced aluminum mirrors for the VUV," *Applied Optics*, 53(4), A125-130 (2013)
[19] "WVASE," https://www.jawoollam.com/ellipsometry-software/wvase (accessed December 2017)
[20] "CompleteEASE Data Analysis Manual," https://crn2.3it.usherbrooke.ca/guide_sb/appareils/Ellipsometre/CompleteEASE%20Manual.pdf (accessed November 2017)
[21] Hilfiker, J.N. et al., "Survey of methods to characterize thin absorbing films with Spectroscopic Ellipsometry," *Thin Solid Films*, 516, 7979-7989 (2008)
[22] Madden, R. P. and Canfield, L.R., "Apparatus for the Measurement of Vacuum Ultraviolet Optical Properties of Freshly Evaporated Films before Exposure to Air," *Journal of the Optical Society of America*, 51(8) 838-845 (1961)